

****Volume Title****

*ASP Conference Series, Vol. **Volume Number***

****Author****

© ****Copyright Year**** *Astronomical Society of the Pacific*

(Sn)DICE: A Calibration System Designed for Wide Field Imagers

N. Regnault¹, E. Barrelet¹, A. Guyonnet¹, C. Juramy¹, P.-F. Rocci¹,
L. Le Guillou¹, K. Schahmanèche¹, F. Villa¹

¹ *Laboratoire de Physique Nucléaire et de Hautes-Energies,
Barre 12-22 1^{er} étage, 4 place Jussieu, 75252 Paris CEDEX 05.*

Abstract. Dark Energy studies with type Ia supernovae set very tight constraints on the photometric calibration of the imagers used to detect the supernovae and follow up their flux variations. Among the key challenges is the measurement of the shape and normalization of the instrumental throughput. The DICE system was developed by members of the Supernova Legacy Survey (SNLS), building upon the lessons learnt working with the MegaCam imager. It consists in a very stable light source, placed in the telescope enclosure, and generating compact, conical beams, yielding an almost flat illumination of the imager focal plane. The calibration light is generated by narrow spectrum LEDs selected to cover the entire wavelength range of the imager. It is monitored in real time using control photodiodes. A first DICE demonstrator, SnDICE has been installed at CFHT. A second generation instrument (SkyDICE) has been installed in the enclosure of the SkyMapper telescope. We present the main goals of the project. We discuss the main difficulties encountered when trying to calibrate a wide field imager, such as MegaCam (or SkyMapper) using such a calibrated light source.

1. Introduction

Modern precision cosmology, such as the measurement of the Dark Energy equation of state with type Ia supernovae (SNe Ia) (see e.g. Sullivan et al. 2011; Conley et al. 2011; Guy et al. 2010; Kessler et al. 2009, and references therein) sets very tight constraints on the accuracy of the flux calibration of the imagers. Indeed, the measurement of the luminosity distance of high-redshift (resp. low-redshift) supernovae is primarily performed with the redder (resp. bluer) bands of the imagers. Hence, measuring cosmological parameters with SNe Ia ultimately boils down to comparing fluxes measured either with red and blue passbands and it is fundamental to control the intercalibration of the imager passbands. Taking full advantage of statistics and quality of SN Ia measurements requires to control this intercalibration with an accuracy of a fraction of a percent.

The current photometric calibration techniques rely on observations of spectrophotometric stellar calibrators. Establishing such primary standards is notoriously difficult, as one has to anchor astronomical observations to a physical flux scale. One of the best efforts so far is the work of the CALSPEC team (CALSPEC 2000, and references therein). The CALSPEC flux scale relies on NLTE *models* of three (and now five) pure hydrogen white dwarfs. These stars are the primary standards used to calibrate the flux response of the HST instruments, in particular STIS and NICMOS, which are used in turn to extend the CALSPEC library by adding secondary spectrophotometric stan-

dards. The SNLS and SDSS-II surveys have chosen to anchor their flux calibration on this so-called HST white dwarf flux scale (Betoule & et al 2012; Regnault et al. 2009; Holtzman et al. 2008). The uncertainty that affects the spectrum of the primary standards is however difficult to assess. As the precision of the calibration efforts improves, it seems increasingly important to check these stellar calibrators using laboratory standards.

The wavelength positioning of the survey passbands has also a sizeable impact on the cosmological parameter measurements, as shown for example in table 9 of Conley et al. (2011). The required wavelength accuracy on the filter cut-offs is as low as a fraction of a nanometer. Passband models are usually derived from pre-installation test-bench measurements of the imager optical components. This is not entirely satisfactory, as filters may evolve over time as shown for example in Doi et al. (2010), and it seems necessary to be able to measure and follow up *in situ* the instrument passbands.

With these requirements in mind, several groups have sought to develop instrumental calibration systems, i.e. light sources that can illuminate the telescope pupil with well characterized light. By today's standards, "well characterized" means that the calibration beam has been mapped using Si photodiodes procured from an institute of standards such as the American Institute of Standards and Technology (NIST). Many different designs have been proposed over the last few years, and quite a few are now being tested on various wide field imagers. In what follows, we describe the DICE system. DICE stands for Direct Illumination Calibration Experiment. It consists in a very stable point-like source, generating conical beams that deliver a quasi-uniform illumination on the focal plane. Two such systems have been built so far. A first prototype was installed at the Canada France Hawaii Telescope (CFHT) in order to calibrate the 1 deg² MegaCam imager. A second generation demonstrator was recently installed in the enclosure of the 5.7 deg² SkyMapper imager. We discuss below the main design (§2) and implementation (§3) aspects of the project. We then describe the test bench procedures that permit to characterize the light source (§4). Finally, we discuss a few key problems that arise in the data analysis (§5).

2. Design Considerations

2.1. Calibration beam

Ideally, a calibration device should mimic as much as possible the science objects under study. Since a supernova survey is dealing primarily with point sources (supernovae and field stars), we should try and generate quasi-parallel beams, covering the entirety of the primary mirror (see figure 1). Such a beam would result in a spot on the focal plane, and we could use the photometry code in production in the survey photometry pipeline to estimate its flux, thereby avoiding the systematic errors that arise from using different flux estimators.

Unfortunately, building a good artificial star turns out to be difficult. For SnDICE, we deliberately opted for a different design, (figure 1). SnDICE is a point source, located in the dome, a few meters away from the telescope primary mirror, close to the object plane. The source generates a conical, quasi-lambertian beam, of aperture $\sim 2^\circ$, slightly larger than the telescope angular acceptance. Such an illumination results in an almost uniform focal plane illumination.

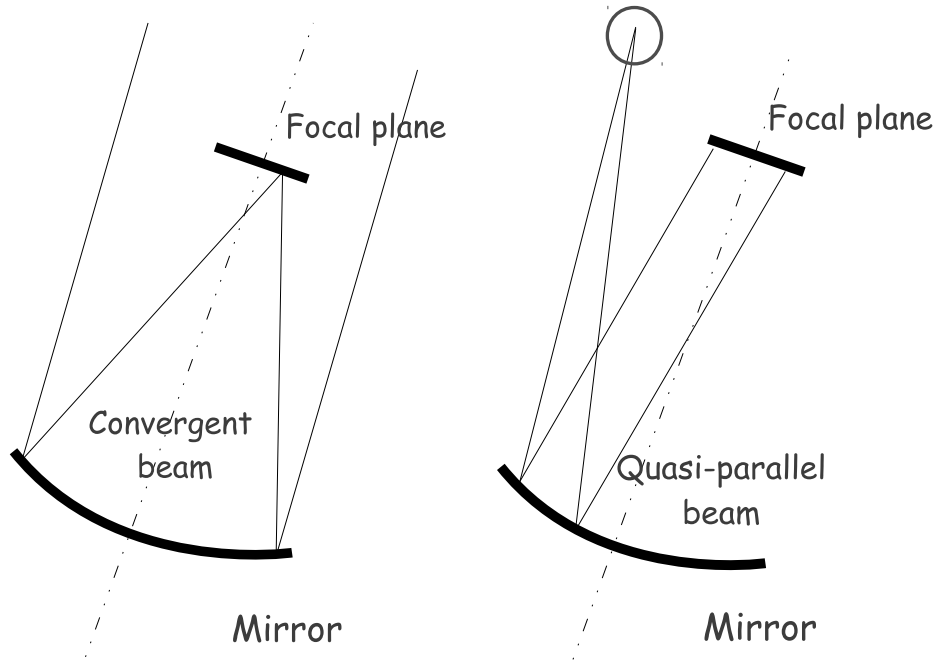


Figure 1. Left: telescope illumination by a point source (“science beam”). Right: SnDICE calibration beam.

As shown on figure 1, the calibration beam is radically different from the science beam. In particular, the angular distribution of the light rays that hit the various optical surfaces (e.g. the interference filters) is not comparable. However, this specific calibration beam has at least one very nice property: it is much simpler than the science beam, in the sense that each pixel sees photons that came through a unique path. In other terms, there is a one-to-one relationship between the focal plane elementary surface elements and the calibration beam elementary solid angles. As we will see, such a property makes it very simple to predict the focal plane illumination, once one knows the beam radian intensity map.

2.2. Light emitters

Another important design element is the choice of narrow-spectrum light emitting diodes (LED) as light emitters. LEDs are known to be extremely stable, as long as they are fed with stable currents. It is relatively easy today to build current sources stable at a few 10^{-5} over a temperature range of a few degrees. Hence, with some care, it is relatively easy to build a light source that can deliver very stable beams over long durations. The diversity of narrow-spectrum LEDs available on the market permits to cover the entire spectral range of silicon imagers, from the near UV to the near infrared (see figure 3).

LED do not emit monochromatic light. The width of typical LED spectra is of about $\delta\lambda/\lambda \sim 5 - 7\%$. Hence, as always, there is a trade-off, as we chose to sacrifice wavelength precision in favor of high-quality and high-stability illumination. This makes sense, since what one actually needs is a *follow-up* more than a *measurement* of the filter cutoff positions. The filter transmissions are indeed well measured prior to installation.

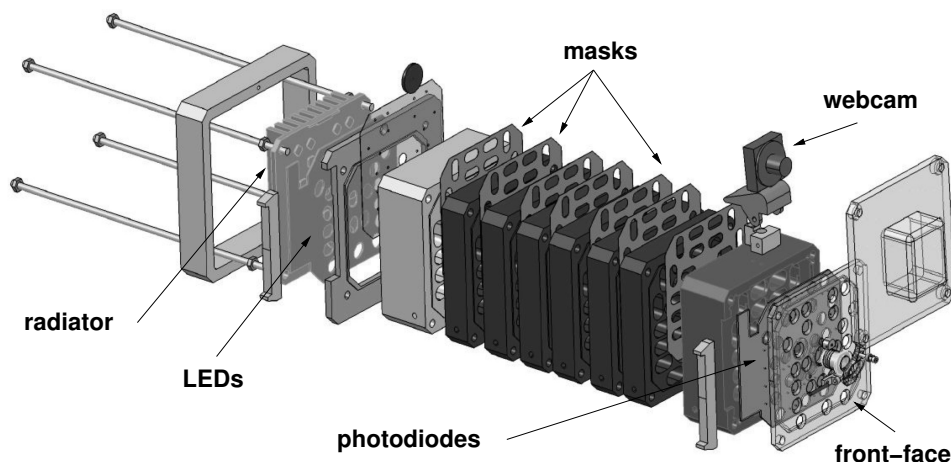


Figure 2. Sketch of the DICE light source. It consists in a modular box, made of 8 (almost) identical aluminum pieces, pierced with holes to let the light through. The LEDs are mounted on a radiator, on the back of the device. Close to the front face, control photodiodes (one for each calibration channel) monitor the light delivered by the LEDs.

LEDs come with just one caveat: their emission properties vary with temperature. As temperature increases, the LED emission efficiency drops by up to $0.5\% / ^\circ \text{C}$, and the mean wavelength of the emitted light shifts redwards by about $0.1 \text{ \AA} / ^\circ \text{C}$. As will be discussed in §4, these variations are generally linear and always extremely reproducible. As a consequence, once each emitter has been well characterized, one only needs to implement a real time follow-up of the source temperature to account for these effects.

3. The DICE System

The SnDICE light source is a $130\text{mm} \times 130\text{mm} \times 300\text{mm}$ box, pierced with 25 asymmetric holes. It contains 24 calibration LEDs mounted on a radiator, located on the back of the device, approximately 260 mm from the front face. The light beams exit through circular apertures of diameter 9-mm. The beams are carefully shaped using a series of masks designed to kill most of the stray light. Off-axis control photodiodes, located close to the front face, monitor in real time the light delivered by each LED. The mechanical design of SkyDICE, the demonstrator installed in the SkyMapper enclosure, is almost identical, except that the LED head is shorter, in order to generate wider (3 degree) conical beams.

Figure 3 shows the quality of the spectral coverage obtained from SnDICE (left) and SkyDICE (right). The LEDs have been chosen so that each filter is sampled by at least three LEDs: one close to the maximum, and two covering the filter cutoffs. As can be seen, the diversity of LEDs available in 2007, at the time SnDICE was designed, does allow to sample well the red cutoff of the MegaCam r filter, as well as the blue cutoff of the i -filter. Also, few LEDs were available in the infrared. Two years later, the diversity of LEDs had dramatically improved, and the spectral coverage provided by SkyDICE is excellent.

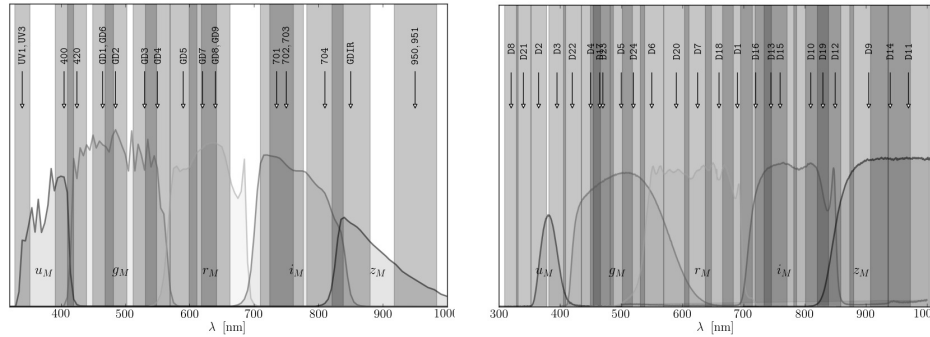


Figure 3. Left: SnDICE spectral coverage of the MegaCam passbands. The arrow indicate the LED central wavelengths $\bar{\lambda}$. The shaded region delimitates the region $0.95\bar{\lambda} < \lambda < 1.05\bar{\lambda}$ to give an idea of the LED spectrum extension. Right: SkyDICE coverage of the SkyMapper passbands.

The source can be oriented using an altitude and an azimuth motor. By moving simultaneously the LED head and the telescope, one is able to scan various locations of the primary mirror, keeping both instruments aligned. A 25th LED called the *artificial planet* is used to control the relative alignment of SnDICE with the telescope. This channel is equipped with a convergent lens that reshapes the light into a (quasi) pencil-beam. Planet exposures display a bright (~ 100 pixel wide) spot, along with a series of *ghosts* generated by reflexions within the telescope optics. The position of the main spot is a direct measurement of the relative orientation of the planet beam and the telescope optical axis. The relative positions of the ghosts encode information on (1) the distance between the planet beam and the telescope optical axis and (2) the alignment of the telescope optics –the WFC lenses, in particular.

The DICE system is designed to deliver very stable beams over long durations. The LEDs are operated at very low currents and should not be subject to significant evolution. Also, there are no intermediate optical surfaces between the emitters and the telescope primary mirror –besides the LED encapsulant. This limits the effect of optical surface ageing. Finally, a set of redundant controls has been implemented: the LED currents and temperatures are monitored in real time, the LED flux is also measured by control photodiodes. Finally, cooled, large area control photodiodes, designed to sense the typical low focal plane illuminations, of a fraction of $\text{nW} / \text{cm}^{-2}$, are placed on the telescope, and provide an additional, independent measurement of the calibration flux delivered by the source.

During a typical data taking session, the dome aperture tracking system is disconnected and the telescope points inside the dome towards the source. The relative alignment and positions of both instruments are controlled with a series of alignment exposures taken with the *planet* beam. Then, sequences of calibration exposures are taken. The source and the telescope are then moved, in order to cover a different mirror area, and the same calibration sequence is repeated. Some calibration sequences are designed to test the repeatability of the readout electronics. They consist in up to 50 exposures taken with the same LED, at regular intervals. The source itself being very stable –and monitored– this allows one to study potential variations of the imager gains over time. Other calibration sequences consist in series of exposures taken with dif-

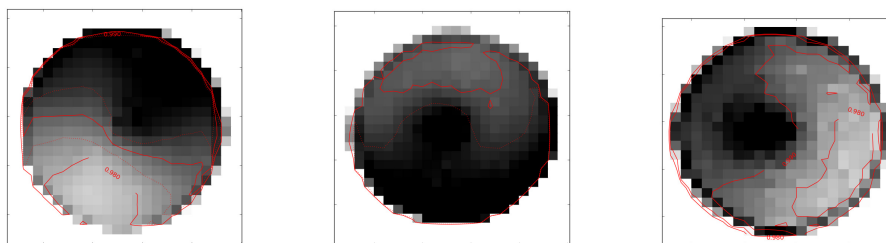


Figure 4. Map of the radiant intensity delivered by three different LEDs, in the blue, green and near UV. The diameter of each beam is of 2 degrees. The non-uniformities shown on the map are of about 1% (peak-to-trough)

ferent LEDs, with and without filter. Such a dataset permits to monitor the telescope transmissions – filter normalization and filter cutoffs.

4. Test Bench Studies

Prior to installation, the light source must be characterized on a spectrophotometric test bench. The goal is (1) to measure the spectral energy distribution of each LED, as a fonction of temperature and (2) to map the beam radiant intensity (in W / sr) – also at various temperatures. All measurements are performed for several values of the LED currents, although, in operations, we try not to vary the LED currents, and adapt the total illumination delivered to the focal plane by varying the exposure time. The nominal current was adapted for each LED, in order to yield a few thousand photoelectrons per pixel and per second on the focal plane.

The test bench is placed in a $2\text{m} \times 2\text{m} \times 3.5\text{m}$ dark enclosure. The enclosure walls are insulated, and its temperature can be regulated from 0°C (typical temperature on site) to 25°C . The bench is not strictly speaking thermalized, as significant temperature gradients can still be measured after a few hours of operations. However, the temperature of all bench elements is monitored using PT1000 thermistors.

The flux measurements are all performed with a calibrated photodiode, purchased from an institute of standards. A very common choice is the 1 cm^2 Hamamatsu 2281, calibrated at the National Institute of Standards and Technology (NIST). Following the recommendations of NIST, it is operated at ambient temperature, in photoelectric mode (not polarized in reverse) and read out using a Keithley 6514 feedback picoammeter. The fluxes measured by the photodiode are of a few nanowatts, yielding photodiode currents of a few nanoamperes (the fluxes recorded by the imager focal plane are about 50 times lower).

The bench operations are fully automated. The LED head and the calibrated photodiode are both mounted on computer controlled linear tables. By moving the photodiode in a plane orthogonal to the head Z-axis one can map the beam radiant intensities. Figure 4 shows three different maps. The beams are not perfectly lambertian, but display small non-uniformities at the level of about 1%. The origin of those non-uniformities, in particular of the central “bump” is unknown. However, they are extremely well measured, with a relative precision of a few 0.01% and do not seem to vary.

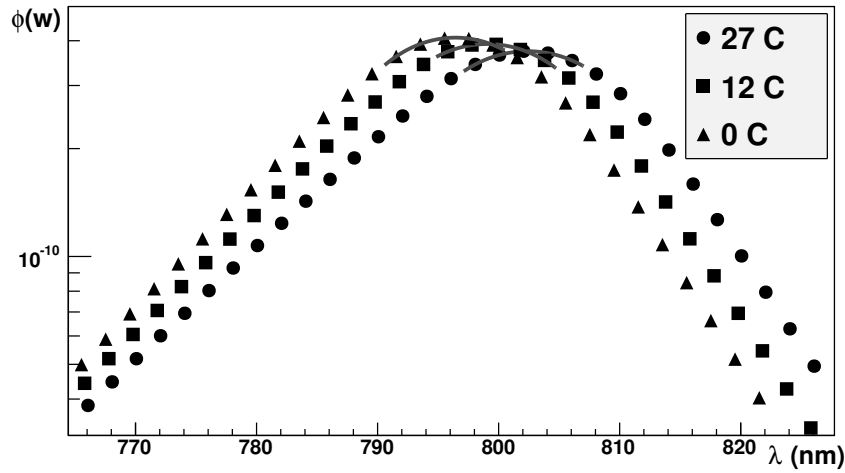


Figure 5. Three spectra of the same LED (810 nm), taken at three different temperatures.

By placing a monochromator (a Digikröm DK240) between the source and the calibrated photodiode one can measure the spectrum of each LED. To do this, the wavelength calibration of the monochromator has to be performed several times over the full temperature range, using Cd and Hg lamps, as small but significant variations of the instrument response with temperature have been found. Taking this into account, the total wavelength uncertainty is of about 1 Å. Figure 5 shows a typical LED spectrum at three different temperatures. The behavior described in §2 is clearly apparent: as temperature decreases, the flux increases and the spectrum is blueshifted. Also, the shapes of the spectra seem to change slightly with temperature.

At the end of the process, we have a full spectrophotometric characterization of the light source. The spectroscopic measurements give the shape of the spectra; the photometric measurements allow one to derive their normalization, as a function of the direction with respect to the source Z-axis. To derive the LED emission properties at any given temperature, we interpolate through the measurements. The fluxes are anchored on the physical flux scale carried by the photodiode. According to NIST, the uncertainties that affect the measurement of the photodiode efficiency are of about 0.2% in the visible ($400\text{nm} < \lambda < 950\text{nm}$). However, NIST does not yet report the correlations between measurements performed at different wavelengths. As a consequence, one cannot compute the uncertainty affecting the relative normalization of LED of different wavelengths without some amount of guessing.

5. Analysis of the Calibration Frames

5.1. Gains & Imager Follow-up

The simplest study that can be done with a DICE system, is to detect and follow-up the short term variations of the imager response – the gains in particular. This has been done using long series of exposures taken with the same LED, taking advantage

of the stability of the light source. Several such studies have been performed with the MegaCam imager. They have shown that most of the 72 readout channels display a stability of about 0.1% (rms), some 5 channels being much more unstable, with a variability of 0.5% to 1%.

DICE can not only study the gain short term temporal variations of the imager response, but also determine with one single exposure, the step-like variations of the imager response, due to the amplifier-to-amplifier gain differences, as well as the CCD-to-CCD quantum efficiency variations. Indeed, the beam radiant intensity being continuous, the focal plane illumination is also continuous. Hence, sharp CCD-to-CCD or amplifier-to-amplifier variations displayed by the calibration frames permit to intercalibrate the CCD and amplifier responses. Hence, performing DICE observations on a regular basis allows to capture the temporal and spatial variations of the imager response (at least the non continuous part of it).

5.2. Flux Measurements

One can expect that the illumination $\phi(\vec{x})$ recorded at a given location \vec{x} on the focal plane when the telescope is illuminated by SnDICE is simply the beam radiant intensity map, multiplied by the response function of the telescope:

$$\phi(\vec{x}) = \mathcal{B}(\vec{u}) \times T(\vec{x}) \times \left| \frac{\partial \vec{x}}{\partial \vec{u}} \right| \quad (1)$$

where $T(\vec{x})$ is the transmission of the telescope, at the LED mean wavelength (i.e. what we are trying to measure), $\mathcal{B}(\vec{u})$ is the radiant intensity emitted in direction \vec{u} by the source (measured on a test bench). Knowing the telescope optics, one can easily compute the geometrical factor $\left| \frac{\partial \vec{u}}{\partial \vec{x}} \right|$, and derive $T(\vec{x})$.

Unfortunately, the situation is slightly more complicated, as the focal plane is also hit by stray light, most of it coming from internal reflections within the telescope wide-field corrector (WFC). The contamination level varies from a few percents to a few per-mil as a function of the focal plane position. Its level depends on the transmissions and reflectivities of the surfaces encountered on the telescope optical path, and also on the curvatures of the various optical surfaces. Hence, the expected flux is rather a sum on all possible paths p that light may follow (yielding non-negligible fluxes):

$$\phi(\vec{x}) = \sum_p \mathcal{B}(\vec{u}) \times T_p(\vec{x}) \times \left| \frac{\partial \vec{x}}{\partial \vec{u}} \right|_p \quad (2)$$

where $T_p(\vec{x})$ is the product of the reflectivities and transmissions encountered by light over its path through the telescope optics. The term $\left| \frac{\partial \vec{x}}{\partial \vec{u}} \right|_p$ encodes the geometrical response of the optics, *for the path p under consideration*. As for direct light, it can be computed using a model of the telescope optics.

We have built a model of the telescope optics, using information provided by the telescope teams. The model itself consists in a raytracer that predicts the impact position on the focal plane, as a function of the incident ray position and orientation, and this, for any chosen light path (i.e. not limited to the direct light). In addition, an empirical focal plane model was built, using the WCS information contained in the science image headers, in order to predict the impact positions in pixels (rather than in millimeters). Finally, the last component of the model –surprisingly the most difficult one

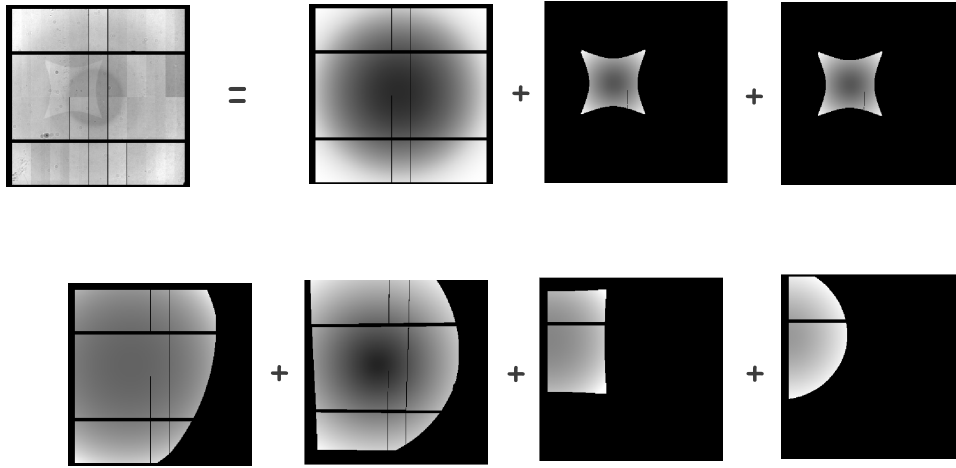


Figure 6. Decomposition of a calibration frame (upper left) into the sum of (1) the direct light (2) ghosts due to the L4, L3 and L2 lenses of the wide field corrector. Note that it is not a Monte-Carlo: we do not propagate photons, but we rather use equations 1 and 2 to directly compute the focal plane illumination.

to build—is a series of geometrical functions that can predict the relative positions and orientations of the source and the telescope with a sufficient accuracy, for any given exposure.

These predictions were tested and tuned on the *planet* exposures, where the ghosts and main spot are well separated. From this, it is relatively easy to compute the expected illumination, for any given ghost. Figure 6 gives an idea on how one can decompose a calibration frame as the sum of a series of contributions, including the direct light and the main ghosts. From this, it is then possible to estimate the contamination of each calibration frame, and to reconstruct the telescope transmission.

Note that the problem discussed above, in particular the challenges posed by contamination by ghosts are, at first order, independant of the light source design. If we were using an extended illumination device, such as a screen, predicting the focal plane illumination would probably be more difficult: first one would have to measure (and follow up) the screen *radiance* (in $\text{W} / \text{sr} / \text{m}^2$); second, to predict the focal plane illumination, one would have to compute an integral over the entire screen, which is computationally much more demanding.

5.3. Applications

Both DICE projects have allowed us to gather very rich calibration datasets whose analysis is still underway. Detailed studies of the imager stability were performed. Preliminary determinations of the MegaCam passbands were obtained. Over the course of this analysis, we have developed accurate models of the instruments (telescope + image). These models were tuned on the *planet* exposures, which gave additional information on the telescope optics (lens positions and reflectivities).

Also, several applications of DICE—not anticipated initially—are currently under study. In particular, it seems that, since DICE permits to estimate the gains of the imager, and to extract the instrument response to the direct light (i.e. to separate the direct light from the ghosts), we can build a ghost-free flat field from a series of DICE expo-

tures. This would be a very useful application. Indeed, for most wide field imagers, the contamination of twilight flats by stray light alters very significantly the uniformity of the instrument response, as discussed for example in Betoule & et al (2012); Regnault et al. (2009).

6. Conclusion

Instrumental calibration is today a very active subject. Many different light source projects have been proposed and it is quite difficult to predict which design is going to prevail in future surveys. DICE is one of those attempts. It consists in a compact, versatile, inexpensive LED based calibrated light source, that can be placed in the dome of virtually any telescope. As a point like source placed at a finite distance, it generates a conical beam that yields a quasi-uniform focal plane illumination. This is complemented by a pencil beam that allows (1) to control the relative positions and orientations of the source and the telescope and (2) to study in detail the ghost contamination. The stability of the light source, permits to carry out a daily monitoring of the telescope and imager response. The simplicity of the calibration beams, combined with the complementarity pencil beam / conical beam allows to derive an accurate estimate of the telescope throughput, taking into account the contamination by stray light.

This project does not address the estimation of the atmospheric transmission, which is an important (and in some bands, highly variable) component of the telescope effective throughput. Many contributions to these proceedings are dealing with this subject.

Acknowledgments. The authors would like to thank the CFHT Corporation and the SkyMapper team for their support. The CFHT staff, in particular Greg Barrick, Jean-Charles Cuillandre, Kevin Ho, Derek Salmon and Jim Thomas provided tremendous amount of help during the installation of the device and the data taking runs that followed. On the SkyMapper side, Brian Schmidt, Peter Conroy, Patrick Tisserand, Annino Vaccarella, and Colin Vest provided invaluable support at all stages of the Sky-DICE project. Finally, we acknowledge support from the LPNHE engineering department, notably P. Bailly, J. Coridian, C. Goffin, H. Lebbolo, A. Guimard, P. Repain, A. Vallereau and D. Vincent.

References

- Betoule, M., & et al 2012, in these proceedings.
 CALSPEC 2000, Calspec, <http://www.stsci.edu/hst/observatory/cdbs/calspec.html>. URL <http://www.stsci.edu/hst/observatory/cdbs/calspec.html>
 Conley, A., Guy, J., Sullivan, M., Regnault, N., Astier, P., Balland, C., Basa, S., Carlberg, R. G., Fouchez, D., Hardin, D., Hook, I. M., Howell, D. A., Pain, R., Palanque-Delabrouille, N., Perrett, K. M., Pritchet, C. J., Rich, J., Ruhlmann-Kleider, V., Balam, D., Baumont, S., Ellis, R. S., Fabbro, S., Fakhouri, H. K., Fourmanoit, N., González-Gaitán, S., Graham, M. L., Hudson, M. J., Hsiao, E., Kronborg, T., Lidman, C., Mourao, A. M., Neill, J. D., Perlmutter, S., Ripoche, P., Suzuki, N., & Walker, E. S. 2011, *ApJS*, 192, 1. 1104. 1443
 Doi, M., Tanaka, M., Fukugita, M., Gunn, J. E., Yasuda, N., Ivezić, Ž., Brinkmann, J., de Haars, E., Kleinman, S. J., Krzesinski, J., & French Leger, R. 2010, *AJ*, 139, 1628. 1002. 3701
 Guy, J., Sullivan, M., Conley, A., Regnault, N., Astier, P., Balland, C., Basa, S., Carlberg, R. G., Fouchez, D., Hardin, D., Hook, I. M., Howell, D. A., Pain, R., Palanque-Delabrouille,

- N., Perrett, K. M., Pritchett, C. J., Rich, J., Ruhlmann-Kleider, V., Balam, D., Baumont, S., Ellis, R. S., Fabbro, S., Fakhouri, H. K., Fourmanoit, N., González-Gaitán, S., Graham, M. L., Hsiao, E., Kronborg, T., Lidman, C., Mourao, A. M., Perlmutter, S., Ripoche, P., Suzuki, N., & Walker, E. S. 2010, *A&A*, 523, A7. 1010.4743
- Holtzman, J. A., Marriner, J., Kessler, R., Sako, M., Dilday, B., Frieman, J. A., Schneider, D. P., Bassett, B., Becker, A., Cinabro, D., DeJongh, F., Depoy, D. L., Doi, M., Garnavich, P. M., Hogan, C. J., Jha, S., Konishi, K., Lampeitl, H., Marshall, J. L., McGinnis, D., Miknaitis, G., Nichol, R. C., Prieto, J. L., Riess, A. G., Richmond, M. W., Romani, R., Smith, M., Takanashi, N., Tokita, K., van der Heyden, K., Yasuda, N., & Zheng, C. 2008, *AJ*, 136, 2306. 0908.4277
- Kessler, R., Becker, A. C., Cinabro, D., Vanderplas, J., Frieman, J. A., Marriner, J., Davis, T. M., Dilday, B., Holtzman, J., Jha, S. W., Lampeitl, H., Sako, M., Smith, M., Zheng, C., Nichol, R. C., Bassett, B., Bender, R., Depoy, D. L., Doi, M., Elson, E., Filippenko, A. V., Foley, R. J., Garnavich, P. M., Hopp, U., Ihara, Y., Ketzeback, W., Kollatschny, W., Konishi, K., Marshall, J. L., McMillan, R. J., Miknaitis, G., Morokuma, T., Mörtzell, E., Pan, K., Prieto, J. L., Richmond, M. W., Riess, A. G., Romani, R., Schneider, D. P., Sollerman, J., Takanashi, N., Tokita, K., van der Heyden, K., Wheeler, J. C., Yasuda, N., & York, D. 2009, *ApJS*, 185, 32. 0908.4274
- Regnault, N., Conley, A., Guy, J., Sullivan, M., Cuillandre, J.-C., Astier, P., Balland, C., Basa, S., Carlberg, R. G., Fouchez, D., Hardin, D., Hook, I. M., Howell, D. A., Pain, R., Perrett, K., & Pritchett, C. J. 2009, *A&A*, 506, 999. 0908.3808
- Sullivan, M., Guy, J., Conley, A., Regnault, N., Astier, P., Balland, C., Basa, S., Carlberg, R. G., Fouchez, D., Hardin, D., Hook, I. M., Howell, D. A., Pain, R., Palanque-Delabrouille, N., Perrett, K. M., Pritchett, C. J., Rich, J., Ruhlmann-Kleider, V., Balam, D., Baumont, S., Ellis, R. S., Fabbro, S., Fakhouri, H. K., Fourmanoit, N., González-Gaitán, S., Graham, M. L., Hudson, M. J., Hsiao, E., Kronborg, T., Lidman, C., Mourao, A. M., Neill, J. D., Perlmutter, S., Ripoche, P., Suzuki, N., & Walker, E. S. 2011, *ApJ*, 737, 102. 1104.1444